

Turbulence driven diffusion in protoplanetary disks – chemical effects in the outer regions

Karen Willacy¹, William Langer¹, Mark Allen^{1,2} & Geoffrey Bryden¹

Karen.Willacy@jpl.nasa.gov

ABSTRACT

The chemistry of the early stages of disk evolution can be used observationally to trace their physical characteristics, but it also determines their later development, including the type and composition of any planets that may form. Modeling can be used in conjunction with molecular observations to understand the extent to which interstellar material incorporated into disks has been processed and can elucidate the nature of the processes acting in the disks. One aspect that has not received much attention until recently is the effect of mixing processes on the observed chemical abundances. The dynamics and chemistry of disks are likely to be intricately linked, with dynamical processes altering the chemical composition and chemistry, in turn, controlling the ionization structure and hence the ability of the magneto-rotational instability to drive disk turbulence. Here we present the results from the first chemical models of the outer regions ($R > 100$ AU) of protoplanetary disks to consider the effects of turbulence driven diffusive mixing in the vertical direction. We concentrate on the outer disk to facilitate comparison with current millimeter and sub-millimeter observations. We show that vertical diffusion can greatly affect the column densities of many species, increasing them by factors of up to two orders of magnitude. Previous disk models have shown that disks can be divided into three chemically distinct layers, with the bulk of the observed molecular emission coming from a region between an atomic/ionic layer on the surface of the disk and the midplane region where the bulk of molecules are frozen onto grains. Diffusion retains this three layer structure, but increases the depth of the molecular layer by bringing atoms and atomic ions formed by photodissociation in the surface layers into the shielded molecular layer where molecules can reform. For other species, notably NH_3 and N_2H^+ , the column densities are relatively unaffected by diffusion.

¹Jet Propulsion Laboratory, California Institute of Technology, Pasadena CA 91109

²Division of Geological Sciences, California Institute of Technology, Pasadena, CA 91125

These species peak in abundance in the midplane, where most other molecules are heavily depleted, rather than in the molecular layer above. Diffusion only affects the abundances of those molecules with peak abundances in the molecular layer. We find that diffusion does not affect the ionization fraction of the disk. We compare the calculated column densities to observations of DM Tau, LkCa 15 and TW Hya and find that good agreement for many molecules with a diffusion coefficient of $10^{18} \text{ cm}^2\text{s}^{-1}$.

Subject headings: stars: formation – stars: planetary systems: protoplanetary disks – ISM: molecules – ISM: abundances

1. Introduction

The collapse of a molecular cloud core to form a star results in the formation of a disk of gas and dust around the young stellar object (YSO) in its center. Observations from the millimeter and infrared probe the gas and dust in the disks and are a primary source of information about their characteristics, providing compositional information as well as details of the density and temperature structure. Chemical processing in the disk affects the molecular abundances and hence what can be observed. The early stages of the disk evolution affect the composition and evolution of the later, planet-forming, stages by determining the nature of the material that is available for coagulation into planets. Understanding this stage of the star and disk formation process is therefore crucial for the understanding of the development of bodies such as are found in our own Solar System.

Most models to date have assumed that the disk is static, e.g. Willacy & Langer (2000); Aikawa et al. (2002); Willacy et al. (2006), or is accreting radially towards the star (Duschl et al. 1996; Bauer et al. 1997; Finocchi & Gail 1997; Finocchi et al. 1997; Willacy et al. 1998; Aikawa et al. 1999; Aikawa & Herbst 1999; Markwick et al. 2002). One process that has not received much attention until recently is how molecular abundances can be affected by mixing processes in the disk. Previous models that have considered such processes, in the radial direction only, were developed by Morfill (1983); Morfill & Völk (1984); Stevenson (1990); Gail (2001); Wehrstedt & Gail (2002). The first study of mixing in the vertical direction was carried out by Ilgner et al. (2004). They found that this process changes the global chemical evolution of the inner 10 AU of a protoplanetary disk. In the protosolar nebula, mixing processes have been shown to be potentially important and may provide a possible explanation of the origin of crystalline silicates in comets (Hanner 1999) and influence the degree of molecular deuteration (Drouart et al. 1999). Considering that protostellar disks are thought to be highly turbulent, with the turbulence influencing their physical evolution, it

seems likely that this could also influence their chemical evolution by providing a mechanism whereby molecules from different parts of the disk can be mixed, driving chemical reactions, and therefore altering the abundances of observable molecules.

Turbulence is a 3-D process and a complete treatment of turbulent driven diffusive mixing would require the inclusion of a full chemical network in a 3-D MHD code. This approach is computationally prohibitive at the present time. Instead insight into the interplay of diffusion and chemistry can be gained by considering a simplified description of the dynamics which allows for a complicated chemical network. Here we present results of 1-D diffusive vertical mixing models in the outer regions ($R > 100$ AU) of a protostellar disk. We chose to study the outer disk because most observations with current instrumentation are sensitive to this region. Our work is therefore relevant to the interpretation of observations of gaseous molecules in T Tauri disks. We consider how the magnitude of the diffusion coefficient affects the predicted column densities and demonstrate that the results are molecule dependent. We find that diffusion is potentially very important, blurring the distinction between the different chemical layers in the disk, and that it will have observable consequences.

2. The diffusive mixing model

Star formation begins with the collapse of a rotating molecular cloud core. This process is very rapid, too rapid to allow the dissipation of angular momentum, since the freefall time is shorter than, or comparable to, the angular momentum transport time (Shu 1995). Collapse therefore often results in either the formation of a system of multiple stars, or of a disk around the young star, or both. Observations have shown that disks are extremely common around young stars. Surveys of the Taurus region indicate that roughly 50% of pre-main sequence stars have disks at an age of 1 Myrs (Strom et al. 1989; Beckwith et al. 1990; Skrutskie et al. 1990; Strom et al. 1993).

Although the evolution of the star–disk system is controlled by angular momentum transport, the mechanism by which this transport is achieved is still unclear. Molecular viscosity is too low to have much of an effect. Partly because disks have a high Reynolds number (much higher than is required in hydrodynamic flows for turbulence to set in), turbulence is thought to be the means by which disks can rid themselves of angular momentum (see Morfill & Völk (1984) and references therein). Several processes have been suggested to drive the turbulence, e.g. the vertical convective instability (Lin & Papaloizou 1980), the magneto–rotational instability (MRI) (Balbus & Hawley 1991; Balbus et al. 1996), the linear Rossby wave instability (Li et al. 2000), the baroclinic instability (Klahr & Bodenheimer

2003; Klahr 2004) and the linear strato-rotational instability (Dubrulle et al. 2005; Shalybkov & Rüdiger 2005). The specific turbulent mechanism is important because it is linked to the physical properties of the disk such as its vertical structure, magnetization, temperature and turbulent velocity dispersion.

Whatever the driving mechanism, a simple method to parameterize the viscous stress in a disk is the α prescription of Shakura & Sunyaev (1973). This describes the angular momentum transport in accretion disks in terms of an ‘anomalous’ viscosity, ν_t , proportional to the gas pressure:

$$\nu_t = \alpha c_s h \tag{1}$$

where c_s is the sound speed, h is the vertical pressure scale height and α is a dimensionless constant (where $\alpha < 1$). The α parameter controls the viscous heating, angular momentum transport and mixing in the disk. Simulations using this prescription can provide the physical parameters (density, temperature, vertical structure) of a disk e.g. d’Alessio et al. (1999, 2001); Bryden et al. (2006). Estimates from the lifetimes of protostellar disks suggest that $\alpha \sim 10^{-2}$ (Calvet et al. 2000), but model values between 10^{-4} and 10^{-1} are commonly used.

The α -disk models have been used to provide the density and temperature structure for many of the current disk chemical models. Various assumptions in the physical parameters have led to quantitative differences in the results from these models. Temperature is especially important as it controls the location of the snow-line – the region where molecules are released from icy grain mantles by thermal desorption. In addition, the chemical evolution is determined by processes such as gas phase two- or three-body reactions, cosmic ray ionization, X-ray and UV irradiation, gas-grain interactions and grain surface reactions. Qualitatively the models are in agreement with a three-layer structure being predicted (Figure 1). In the cold midplane molecules are mainly accreted onto the dust grains, with little remaining in the gas apart from H_2 and its ions. At the surface of the disk, the gas is warmed by irradiation from the central star. Here molecules can be thermally desorbed from the mantles and, once in the gas, are quickly photodissociated by the strong UV field from both the interstellar medium and from the star. Between these two layers is a region which is shielded from the external UV but where molecules can be kept in the gas and prevented from complete freezeout by desorption processes, either thermal or non-thermal. There is still a great deal of debate as to which non-thermal processes might be acting. Here we include thermal desorption and cosmic ray heating of grains but ignore other non-thermal processes in order to concentrate on the effects of diffusion alone.

The diffusive mixing model used here was initially developed to model the chemistry of planetary atmospheres (Allen et al. 1981). It also has been used by us to model molecular cloud chemistry (Xie et al. 1995; Willacy et al. 2002). The method assumes that the turbulent

diffusion timescale for a given tracer depends on its composition gradient. If the disk is divided up into a series of zones, then diffusion will only occur between two adjacent zones if there is a composition gradient between them. If the transport timescale between the zones is less than the chemical timescale then the chemistry will be coupled to the turbulent diffusion.

In 1-D the problem can be parameterized as follows (Allen et al. 1981). We assume that $n(\text{H}_2)$ is the number density of H_2 , n_i is the number density of molecule i and x_i is the fractional abundance of i ($= n_i/n(\text{H}_2)$). Using mixing length theory (which characterizes turbulence as eddies that maintain different properties to the average fluid in which they exist for the time taken to travel a distance l - known as the mixing length), we can approximate fluctuations in the fractional abundance, δx_i , due to the turbulence as

$$\delta x_i = -l \frac{dx_i}{dz} \quad (2)$$

where dx_i/dz is the abundance gradient in the z -direction. The net transport flux of i is then given by

$$\begin{aligned} \phi_i &= n(\text{H}_2) \langle v_t \delta x_i \rangle \\ &= -K n(\text{H}_2) \frac{dx_i}{dz} \\ &= -K n_i \left(\frac{1}{n_i} \frac{dn_i}{dz} - \frac{1}{n(\text{H}_2)} \frac{dn(\text{H}_2)}{dz} \right) \end{aligned} \quad (3)$$

where K is the diffusion coefficient, defined as $K = \langle v_t l \rangle$ and v_t is the turbulent velocity. Using this description of 1-D diffusion, we can write the chemical continuity equations as

$$\frac{\partial n_i}{\partial t} + \frac{\partial \phi}{\partial z} = P_i - L_i \quad (4)$$

where P_i and L_i are the chemical production and loss terms for species i , respectively. The diffusion–chemistry code solves the coupled continuity equations for all species simultaneously by first linearizing it around an initial guess. The subsequent linear parabolic partial differential equations are solved using a completely implicit finite difference method described by Richtmeyer (1957) (pp101-105, this scheme is not in the later edition). It can be shown that the numerical solutions converge as (Δt) and $(\Delta z)^2$. The solution is iterated until the absolute fractional errors are less than 10^{-4} . A similar method was used by Strobel & McElroy (1970) for modeling the F2 layer in the terrestrial atmosphere. In this paper calculations are carried out with a vertical spacing of 2 AU, so the number of zones varies with radius.

We assume that there is no infall into the disk, an assumption that is appropriate for the T Tauri phase where accretion is of less importance than in the earlier stages of the star

formation process. We also assume that material cannot escape through the outer boundary, so the total flux across it is zero. We assume that the other boundary is the midplane, and again no flux crosses this boundary.

2.1. Determining the diffusion coefficient

A critical factor in our model is the choice of diffusion coefficient, K . We can define reasonable values of the diffusion coefficients if the mixing process responsible for the diffusion of chemical species is also responsible for the dispersion of angular momentum. In this case we can estimate the diffusion coefficient from the viscosity and hence $K = \nu_t = \alpha c_s h$. This approach has been used previously by several authors, e.g. Morfill (1983); Morfill & Völk (1984); Stevenson (1990); Gail (2001); Wehrstedt & Gail (2002) to model the radial transport in disks.

We assume that the gas and dust are well mixed and that the dust grains are small enough that they experience mixing with the same diffusion coefficient as the gas. Grains whose stopping times are less than the orbital period are likely to diffuse with the gas. Under the conditions in our disk this means that grains with radii up to several tens of centimeters will move with the gas. The transport of grains from midplane to the heated surface regions means that desorption from grains can potentially provide a source of molecules, atoms and ions in the upper regions of the disk. This will be discussed in our results below. One limitation of our model is that the mixing of a given species is calculated based on its concentration gradient. Thus the mantle species, rather than the grain itself, are assumed to diffuse. This will be addressed in future work.

Recent work by Johansen & Klahr (2005) has measured directly the turbulent diffusion coefficient of dust grains embedded in an MHD disk model and compared this to the turbulent viscosity of the flow. They found that the Schmidt number ($S_C = \nu_t/K$) is about 1.5 in the vertical direction and 0.8 radially. However these results do not agree with those of Carbadillo et al. (2005) who found $K \sim 0.1 \nu_t$. More work is required to determine the correct value. In the meantime, we have elected to assume that $S_C = 1$, i.e. $K = \nu_t$.

Assuming $K = \nu_t$ we can find a typical value of K in our disk. At a radial distance of 100 AU from the star, our disk model has a gas temperature of 75 K at the surface giving $c_s = 4.4 \times 10^4 \text{ cms}^{-1}$. Taking $h/R = 0.15$ and $\alpha = 10^{-2}$ we find $K = 9.9 \times 10^{16} \text{ cm}^2\text{s}^{-1}$. Because of the uncertainties in estimating K , and because changing α could alter K by orders of magnitude, (disk models use values of α between 10^{-4} and 10^{-1}), we have chosen to test the effects of diffusion on chemistry by considering values of K between 0 and 10^{18}

cm^2s^{-1} . We also make the simplifying assumption that K does not vary with position in the disk. This spread of diffusion coefficients will be sufficient to show us whether or not diffusion affects the chemistry in the outer disk and how strong the mixing needs to be to have observable consequences.

3. The disk model

The disk model used here is that of Bryden et al. (2006). This model describes the structure of a geometrically thin, flared, disk which is heated both viscously and by radiation from the central star. The model assumes that the disk is in steady state, i.e. that the disk properties are independent of time and that there is a constant mass accretion rate. The structure of the disk is determined by solving the hydrodynamical equations semi-analytically.

The model we use has a mass accretion rate $= 10^{-8} M_{\odot} \text{ yr}^{-1}$. The central star has a mass of $0.7 M_{\odot}$, temperature $T_* = 4000 \text{ K}$, and radius $R_* = 2.4 R_{\odot}$. The parameter α is set at 0.01. The surface density is $\Sigma_0 = 1000 \text{ g cm}^{-2}$ at 1 AU and the density varies with radius as $\rho(R) \propto R^{-3/2}$ for $R > 16 \text{ AU}$. The bulk opacity of the disk has two values only: one to visible starlight ($\kappa = 0 \text{ cm}^2\text{g}^{-1}$ in the upper atmosphere) and one to its own infrared radiation ($\kappa = 2 \times 10^{-4} T^2 \text{ cm}^2\text{s}^{-1}$ within the disk). This is a similar approach to that taken by Chiang & Goldreich (1997). The grain size distribution is assumed to follow an equilibrium cascade power-law, $da/dn \propto a^{-3.5}$, such that the mass is concentrated in the largest particles, while the area (and hence the opacity) is dominated by the smallest particles. This more closely resembles a Pollack distribution (Pollack et al. 1994), rather than a small-grain interstellar population. The mean molecular weight is 2.35. The disk structure is calculated between radii of 0.05 and 500 AU and from 0 to $\pi/4$ in meridional angle. The total disk mass in this domain is $\sim 0.05 M_{\odot}$.

The calculated density and temperature structure from this model are shown in Figure 2. We assume that the gas temperature is the same as the grain temperature. In reality, this probably underestimates the gas temperature in the surface layers (Kamp & Dullemond 2004). As has been seen in previous models, the temperature structure of the disk can critically affect the molecular distributions in the disk by controlling the regions where thermal desorption occurs. The grain temperature distribution in our model is consistent with that calculated by d’Alessio et al. (2001) although somewhat colder than in previous models by d’Alessio et al. (1999). The reduction in temperature arises from the different assumptions about the grain size distribution. Both d’Alessio et al. (2001) and Bryden et al. (2006) assume that some grain coagulation has taken place so that the grain size distribution is

closer to a Pollack distribution than the interstellar grain distribution assumed to d’Alessio et al. (1999). These colder disk models have been found to be in better agreement with the observed SEDs of disks.

4. Chemistry

4.1. Reaction set and input abundances

The chemical model is a subset of the UMIST RATE95 database (Millar et al. 1998). We have followed the chemistry of 79 gas phase and 31 ice species (containing H, He, C, N, O and Si), linked by 1480 reactions. The full species set is listed in Appendix A. The chemistry includes thermal desorption, ionization (from the interstellar radiation field and the star, and from the decay of radioactive isotopes), and gas–grain interactions, including surface reactions and thermal desorption. These processes are discussed in more detail below.

To take into account the fact that material incorporated into the disk has already undergone processing in the parent molecular cloud we take the input abundances to the disk model from the output of a molecular cloud model that has been allowed to run for 1 Myrs. The input abundances for the cloud model are given in Table 1. We assume all elements are in their atomic form (or ionic in the case of carbon), with the exception of hydrogen which is 99% molecular. The cloud model is run with a density of $2 \times 10^4 \text{ cm}^{-3}$, at a temperature of 10 K and with a visual extinction of 10 magnitudes. The species and reaction sets used are the same as for the the disk model. Ionization is provided by cosmic rays, photons and cosmic ray induced photons, and freezeout and desorption (thermal and cosmic ray heating of grains) is included. This results in a mixture of gas and ice at 1 Myrs. The abundances of the major species at this time are listed in Table 2 and these are used as inputs to the disk models discussed below.

4.2. Ionization processes

Several processes contribute to ionization in the disk. As in molecular clouds, cosmic rays can cause ionization if the surface density is low enough for them to penetrate (cosmic rays can penetrate densities up to 150 gm^{-2} (Umebayashi & Nakano 1981)). This is always the case in the region of disk considered here. Indirectly, cosmic rays are responsible for a UV photon field which can cause photodissociation Prasad & Tarafdar (1983). Cosmic rays ionize H_2 , generating secondary electrons with an energy of $\sim 30 \text{ eV}$. These electrons can excite electronic states of H_2 which then decay producing a UV flux.

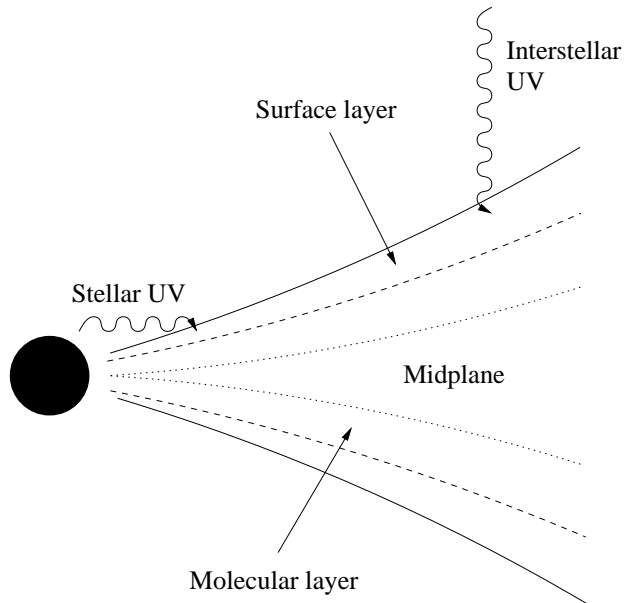


Fig. 1.— Schematic of the chemical structure of a protostellar disk showing how the disk can be divided up into three chemically distinct layers.

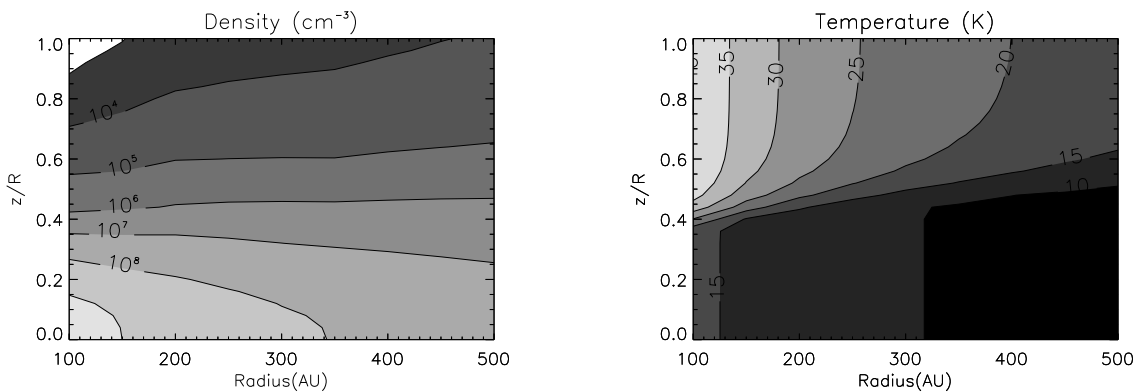


Fig. 2.— The physical structure of a disk calculated using a hydrodynamical model of a geometrically thin disk heated both viscously and by irradiation from the central star. The equations are solved semi-analytically. The disk is assumed to be in steady state. The mass accretion rate is $10^{-8} M_{\odot} \text{ yr}^{-1}$, $\alpha = 0.01$, $\Sigma_0 = 1000 \text{ g cm}^{-2}$ at 1 AU (Bryden et al. 2006). *Left Panel:* Number density profile. Contours run from 10^3 to 10^9 cm^{-3} . *Right panel:* Grain temperature (assumed to be equal to the gas temperature). Contours are at 10, 15, 20, 30, 40, 50, 60 and 70 K.

UV photons from both the star and the interstellar radiation field can cause ionization in the disk. We estimate the UV field at any given position in the disk by assuming that interstellar photons hit the disk vertically and that stellar photons travel horizontally. The strength of the stellar UV field for a T Tauri star has been estimated as 10^4 times the interstellar radiation field at 100 AU by Herbig & Goodrich (1996) and more recently as a few hundred times the interstellar radiation field at 100 AU by Bergin et al. (2003). Here we have chosen to use a value of 500 times the interstellar radiation field following Bergin et al. In common with Aikawa et al. (2002), we have assumed that the stellar radiation field does not dissociate CO and H₂, although these molecules are dissociated by the interstellar radiation field. We use the approach of Lee et al. (1996) to describe the self-shielding of these molecules.

The decay of radioactive isotopes can be a source of ionization in the disk (Umebayashi & Nakano 1981). ²⁶Al can decay to form excited ²⁶Mg which in turn decays by positron decay or by electron capture. We include the ionization due to these decays using the rate found by Umebayashi & Nakano (1981) i.e. $\zeta_R = 6.1 \times 10^{-18} \text{ s}^{-1}$.

T Tauri stars can have strong X-ray fields. Igea & Glassgold (1999) modeled the effects of X-ray ionization in the disk and found that it is effective for $R < 10$ AU. It is most effective in the surface layers because the attenuation length of X-rays is very small. Aikawa & Herbst (2001) included X-rays but found that they did not significantly alter the results for the outer disk. Since we are considering only $R > 100$ AU we have chosen to ignore the effects of X-rays.

4.3. Gas–grain interactions and grain surface chemistry

We assume that all species can freezeout onto grains. The exception is He which has such a low binding energy (100 K; Tielens & Hagen (1982)) that it is easily desorbed even at very low temperatures. We therefore assume that He is not affected by collision with grains and any He⁺ that collides with a grain is neutralized and returned to the gas. For all other species the freezeout rate is given by

$$k_f = S_x < \pi a^2 n_g > C_i v_x n_x \quad (5)$$

where S_x is the sticking coefficient (assumed to be 0.3 for all species), a is the grain radius, n_g is the number density of the grains, v_x is the gas phase velocity of species x and n_x is the number density of x . We assume $< \pi a^2 n_g > = 2.1 \times 10^{-21} n_H \text{ cm}^{-1}$, and $n_g = 10^{-12} n_H \text{ cm}^{-3}$. C_i is a factor that takes into account the effect of charge on the freezeout rate. Umebayashi & Nakano (1980) showed that the majority of grains in dense regions

are negatively charged. Hence the accretion rate of a positively charged ion is enhanced compared to that of neutrals and C_i is given by

$$\begin{aligned} C_i &= 1 \quad \text{for neutral species} \\ &= 1 + e/(akT) \quad \text{for single charged positive ions} \end{aligned} \quad (6)$$

where e is the electron charge and k is the Boltzmann constant. (We do not explicitly track the grain charge, but instead following Umebayashi & Nakano (1980) assume that the grains on average have a negative charge). Ions that hit a grain are neutralized in the same way that they would be if they reacted with an electron in the gas.

Reactions between grain–surface species are included. We assume that only atoms are able to freely move across the grain surface, larger species are prevented from moving because of their higher binding energies. Therefore all grain surface reactions involve at least one atom.

The rate equation method is still the most tractable means of modeling the combined gas and grain chemistry. However, it is known to be flawed because it does not take into account the discrete nature of grains, with potentially significant effects on the calculated abundances. It has been shown that the results for a rate equation calculation of the ice composition can differ markedly from those of a Monte Carlo model (Charnley 1997; Tielens & Charnley 1997; Caselli et al. 1998). One way around this is to reduce the scan rate of hydrogen atoms across the surface of a grain, thus reducing their reaction rate, and bringing the results of the two methods into better agreement. Recent experimental work by Katz et al. (1999) has suggested that the scan rate of hydrogen atoms is much lower than was generally assumed. Ruffle & Herbst (2000) found that a rate equation model using the scan rates of Katz et al. (1999) gives better agreement with the Monte Carlo models, than do models which utilize the fast scan rate. Here we have chosen to follow Ruffle & Herbst (2000) in using the binding energy data of Katz et al. (1999) to calculate the grain surface reaction rates. The binding energy data used is given in Table 3.

The grain surface reaction set is taken from Hasegawa & Herbst (1993). The rates are assumed to be temperature dependent and are calculated as follows. The scan rate of an atom can be calculated from

$$t^{-1} = \nu_0 \exp(-E_b/kT_{gr}) \quad (7)$$

where ν_0 is the frequency of oscillation between adsorbate and surface, given by

$$\nu_0 = \sqrt{(2n_s E_D / \pi^2 m)} \quad (8)$$

where n_s is the surface density of sites ($\sim 1.5 \times 10^{15} \text{ cm}^{-2}$), E_D is the binding energy of the atom, m its mass, $E_b = 0.3 E_D$ and T_{gr} is the grain temperature.

Molecules in the ice mantle are returned to the gas phase by thermal desorption and by desorption due to cosmic ray heating of grains. The rates for thermal desorption are calculated using the binding energies listed in Table 3. The rates for cosmic ray heating are calculated using the method of Hasegawa & Herbst (1993). We find that for the majority of species cosmic ray heating is not an important process. The exceptions to this are those molecules which are relatively weakly bound e.g. N_2 .

5. Results

The effects of diffusion on the calculated fractional abundances and column densities depends on the position in the disk and on the molecule under consideration. Figure 3 shows the calculated column densities at 1 Myrs for several important molecules and illustrates how some molecules are greatly affected by the inclusion of diffusion, whereas others, notably N_2H^+ and NH_3 are relatively unaffected. The effect increases with increasing K , and the column densities for $K = 10^{16} \text{ cm}^2\text{s}^{-1}$ are very similar to $K = 0$ for $R > 200 \text{ AU}$. The effect is increased at smaller R because of the higher disk temperature which increases the abundance of molecules in the gas as a result of thermal desorption. For $K = 10^{18} \text{ cm}^2\text{s}^{-1}$ a similar radial effect is seen.

In general, diffusion smooths out abundance variations with z (as expected) and increasing the depth of the molecular layer (Figures 4 and 5). The chemical effects induced by diffusion arise both from the transport of icy grains from the cold midplane into a warmer region, where the ices can be desorbed, and by the movement of atoms and ions from the highly irradiated surface layer into more shielded regions where molecules can form and survive. Molecules in the diffusion models are formed by the same reactions as in the no diffusion case, but the abundances can be increased because of the increase in potential reactants.

Most molecules exist in a layer between the cold midplane and the UV irradiated surface region (Figure 1). Exceptions to this are N_2H^+ and NH_3 which have peak abundances in the midplane. The upper bound of the molecular layer is determined by photodissociation effects, and the lower one by the point where freezeout dominates the formation processes. For molecules in this layer, the transport of atoms and their ions from the surface is important in driving the chemistry. Diffusion brings atomic and ionized carbon, nitrogen and oxygen into the molecular layer, increasing the formation rate of molecules such as CO , H_2O and CH_4 . These form in the gas phase by the same ion-molecule reaction routes as are found in molecular clouds. For CN and HCN however, neutral–neutral reactions are important:





The usual gas phase reaction formation via HCNH^+ is only important in the $K = 0 \text{ cm}^2\text{s}^{-1}$ case where it is comparably efficient to the neutral–neutral processes.

We consider CO to illustrate how diffusion alters the chemistry. $N(\text{CO})$ increases with K for all radii. The same reactions form and destroy this molecule in all models, CO is formed by thermal desorption and destroyed by freezeout in the midplane region, and by photodissociation in the outer layers. The changes in column density are due to the effects of diffusion which broadens the depth of the molecular layer and increases the peak fractional abundance (Figure 4). The transport of icy grains towards the surface ensures that there is a continual source of CO in the diffusion models, leading to higher CO fractional abundances and a broader high abundance region. At 100 AU the peak abundance of CO occurs at $z = 40$ AU. For $z > 40$ AU thermal desorption ensures that the grains are free of CO ice. In this region there is an additional contribution to the CO from gas phase chemistry for $K = 10^{18} \text{ cm}^2\text{s}^{-1}$ from the dissociative recombination of HCO^+ . Similar effects are seen at other radii (Figure 5).

Water is another molecule whose column density is increased by diffusion. In this case the oxygen chemistry is driven by the transport of grains into the warm surface region where O_2 ices can desorb. O_2 can form efficiently on the grains near the surface in regions where oxygen atoms are plentiful but the hydrogen is mainly tied up in H_2 . Photodissociation of O_2 can then produce oxygen atoms which are transported in turn into the molecular layer. Another source of oxygen atoms is the photodissociation of CO. The direct desorption of water ice is not a good source of gas phase water as the temperature is too low for thermal desorption to occur at the disk radii considered here.

N_2H^+ and NH_3 differ from many other species in that they have high midplane abundances. They also show little variation in column density with diffusion. Both molecules are derived from N_2 (N_2H^+ forms from the reaction of N_2 with H_3^+) whereas NH_3 is formed by a chain of reactions starting from the breakup of N_2 into N^+ and N atoms by reaction with He^+ . N_2 is very volatile and can be desorbed even in the midplane (either by thermal desorption or by cosmic ray heating). It therefore cycles back and forth between the gas and solid phases. Diffusion means that both gas and solid N_2 are transported, spreading out the molecules so that the peak abundance falls, and the vertical extent of the N_2 layer is increased slightly. Hence we see some small changes in the vertical fractional abundance distribution, but relatively little change in the column densities.

The ionization fraction $x(e)$ is not significantly affected by diffusion. At 100 AU we find $x(e) = 2.5 \times 10^{-11}$ for models with both $K = 0$ and $K = 10^{18} \text{ cm}^2\text{s}^{-1}$. At 300 AU the ionization fraction is 1.45×10^{-10} for $K = 0$ and 2.0×10^{-10} for $K = 10^{18}$. At 500 AU a

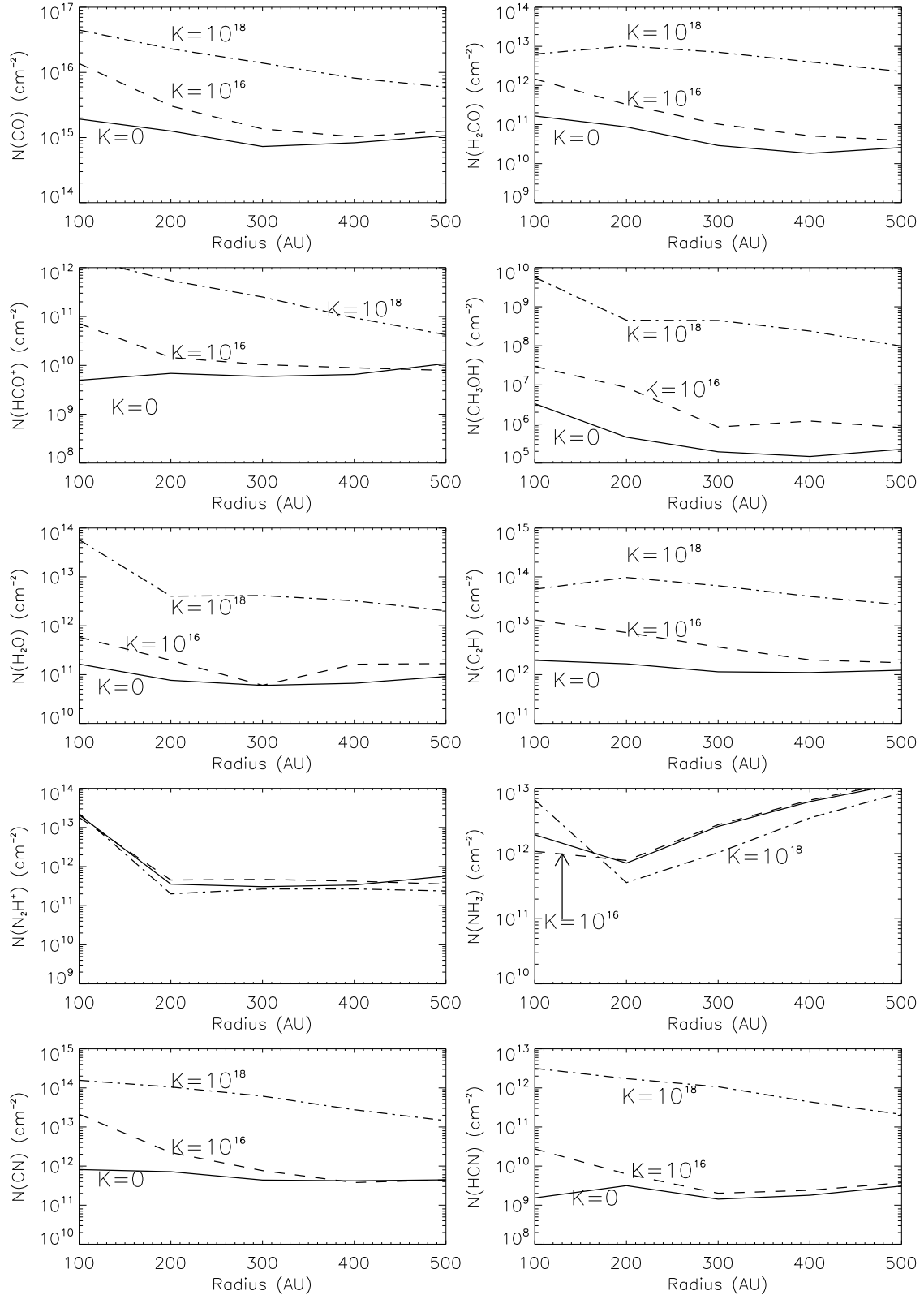


Fig. 3.— Radial distribution of the column densities through the disk for several molecules at a model time of 1 million years. The solid lines indicate $K = 0 \text{ cm}^2\text{s}^{-1}$, dashed lines are for $K = 10^{16} \text{ cm}^2\text{s}^{-1}$ and dash-dotted lines are for $K = 10^{18} \text{ cm}^2\text{s}^{-1}$. These figures show that diffusion increases the column densities of most species. The exceptions are NH_3 and N_2H^+ , which are depleted in the outer disk.

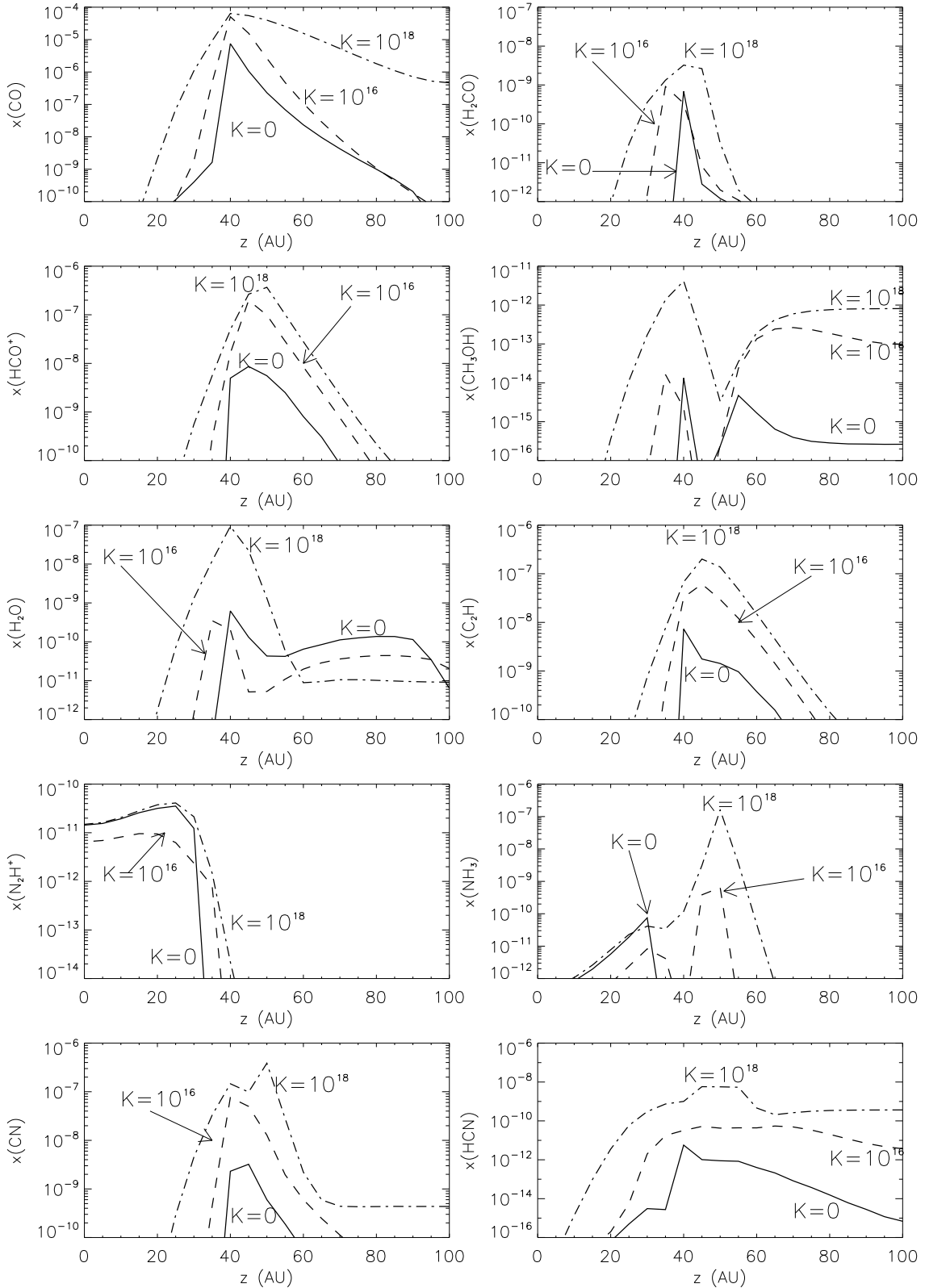


Fig. 4.— Fractional abundances with respect to H₂ as a function of height z above the midplane for $R = 100$ AU and a model time of 1 million years. The solid lines indicate $K = 0$ cm²s⁻¹, dashed lines are for $K = 10^{16}$ cm²s⁻¹ and dash-dotted lines are for $K = 10^{18}$ cm²s⁻¹. Diffusion increases the peak abundance and the vertical extent of many molecules. Arrows indicate N₂H⁺ and NH₃ which are the only molecules that are not detected in the observations.

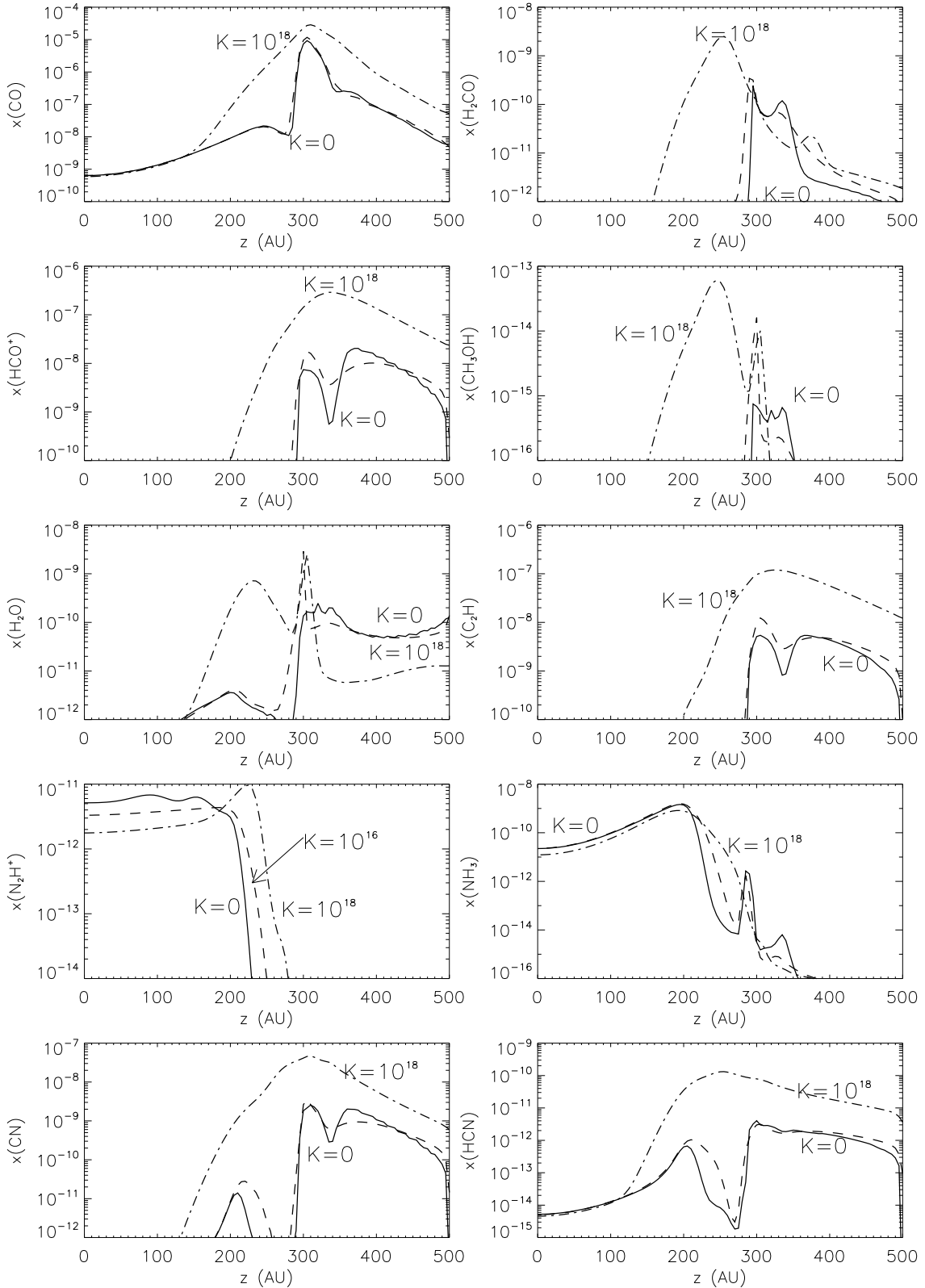


Fig. 5.— Fractional abundances as a function of height z above the midplane for $R = 500$ AU and a model time of 1 million years. The solid lines indicate $K = 0 \text{ cm}^2\text{s}^{-1}$, dashed lines are for $K = 10^{16} \text{ cm}^2\text{s}^{-1}$ and dash-dotted lines are for $K = 10^{18} \text{ cm}^2\text{s}^{-1}$. At this radius $K = 10^{18} \text{ cm}^2\text{s}^{-1}$ is required to affect the abundances and to increase their peak values and the

slight decrease in $x(e)$ from 7.9×10^{-10} to 6.3×10^{-10} is seen when diffusion is included. Recent observations by Ceccarelli et al. (2004) have estimated $x(e)$ in the midplane of a disk and we compare our results to these observations below.

In summary, most molecules show an increase in column density with increasing diffusion. Those with peak abundances that lie near the midplane (e.g. molecules such as NH_3 and N_2H^+ which can remain in the gas even after other molecules are heavily depleted), are least affected by diffusion. Those molecules that peak in the molecular layer (Figure 1) are affected by the transport of ices into the warmer layers where they can be desorbed and photodissociated and returned as reactive atoms and ions to the molecular layer, where they can drive the chemistry. Our models indicate that N_2H^+ and NH_3 are important tracers of the midplane conditions and dynamics in the outer disk. As the radius decreases NH_3 moves into the molecular layer, but N_2H^+ remains in the midplane (see Figures 4 and 5).

5.1. Comparison to observations

We present a comparison of our results with available observations of the outer parts of the disks around the T Tauri stars, DM Tau, LkCa 15 and TW Hya. DM Tau is located 140 pc away in Taurus; with an age of ~ 5 Myrs, it is one of the oldest T Tauri stars. It has a stellar mass of $0.55 M_\odot$ (Simon et al. 2000) and a temperature of 3720 K (Guilloteau & Dutrey 1998). The disk itself has a gas mass of $0.03 M_\odot$ (Guilloteau & Dutrey 1998), a radius of ~ 800 AU (Simon et al. 2000), and a mass accretion rate is $10^{-8} M_\odot \text{ yr}^{-1}$ (Hartmann et al. 1998). LkCa 15 is also located in Taurus. The star has a mass of $1 M_\odot$ (Simon et al. 2000) and a temperature of 4365 K (Muzerolle et al. 2000). The disk radius is slightly smaller than that of DM Tau at 650 AU (Simon et al. 2000) and it has a mass accretion rate of $10^{-9} M_\odot \text{ yr}^{-1}$ (Hartmann et al. 1998). The age has been variously estimated at 3–5 Myrs (Simon et al. 2000) to 12 Myrs (Thi et al. 2001). TW Hya is a classical T Tauri star with a nearly face on disk at ~ 56 pc (Webb et al. 1999). Its age is ~ 15 Myrs and its mass accretion rate is $\sim 10^{-8}$ (Kastner et al. 2002).

The column densities derived from observations are very sensitive to assumptions made about the source. Single dish observations cannot resolve the disks and assumptions about the density and temperature structure of the disks must be made, in order to determine abundances and column densities. For DM Tau Dutrey et al. (1997) determined the gas density distribution of a geometrically thin disk in hydrostatic equilibrium and used this to derive the average fractional abundances with respect to H_2 , assuming that the fractional abundances were the same everywhere in the disk. Aikawa et al. (2002) used the model and data from Dutrey et al. (1997) and integrated vertically to determine the column densities

quoted in Table 4. For LkCa 15 both single dish and interferometric data is available. Qi (2001) used the Owens Valley Radio Interferometer (OVRO) array to observe this source and derived beam average column densities. The resolution of the array (~ 300 AU at the distance of LkCa 15) is such that the source is just resolved. Thi et al. (2004) present single dish observations of LkCa 15. They derive the column densities assuming that the radius of the disk is 450 AU. The disk radius can have a large effect on the calculated column densities with a change from R_1 to R_2 scaling the column densities by $(R_1/R_2)^2$. The single dish column densities are significantly higher than those from the interferometer data due to the differences in the assumptions used to determine these numbers.

Given the uncertainties in both the models and the derivation of column densities from the observations, our model results for $K = 10^{18} \text{ cm}^2\text{s}^{-1}$ are in remarkably good agreement with the observations of DM Tau. We find good agreement (defined as the column densities from the model and observations agreeing to within a factor of 5) for all observed molecules in this source. For Lk Ca 15 we are able to match the single dish observations, but have less success with the interferometric data, which tend to result in much larger column densities. Consequently our $K = 10^{18}$ model is unable to account for the column densities of HCN, CH_3OH and HCO^+ , although we find good agreement for the other molecules. For TW Hya, our $K = 10^{18}$ model does not produce sufficient HCN or HCO^+ , and overproduces H_2CO .

CH_3OH has been detected in LkCa 15 by Qi (2001) using OVRO with a column density of $7.3 \times 10^{14} - 1.8 \times 10^{15} \text{ cm}^{-2}$. Thi et al. (2004) found an upper limit for $N(\text{CH}_3\text{OH})$ in the same source of $< 9.4 \times 10^{14} \text{ cm}^{-2}$. H_2CO has also been observed in LkCa15 and the column density is estimated to be $1.0 \times 10^{14} \text{ cm}^{-2}$ by Thi et al. (2004) or $7.2 \times 10^{12} - 1.9 \times 10^{13} \text{ cm}^{-2}$ by Aikawa et al. (2003). Our model value of $N(\text{H}_2\text{CO}) = 7.1 \times 10^{12}$ at $R = 300$ AU for $K = 10^{18} \text{ cm}^2\text{s}^{-1}$ is in agreement with the observations in this source, but we are unable to account for the observed $N(\text{CH}_3\text{OH})$. Both H_2CO and CH_3OH are thought to form on the surfaces of dust grains by the hydrogenation of CO, although the exact mechanism and the reaction rates are still a matter of debate (Watanabe & Kouchi 2002; Hiraoka et al. 2002). Due to the lack of consensus on the rates we have not included the formation of CH_3OH on grains, although we do have formation of H_2CO from hydrogenation of CO with an activation barrier of 1000 K. This results in the formation of a small amount of H_2CO on the grains. Diffusion increases the column density of both molecules, with a slightly greater effect on CH_3OH . The inclusion of grain formation reactions for CH_3OH would increase its column density somewhat but its high binding energy ($E_b(\text{CH}_3\text{OH}) = 4240$ K: Sandford & Allamandola (1993)) means that it is not easily returned to the gas unless there is a non-thermal desorption process acting. The lower binding energy of H_2CO compared to CH_3OH also means that it is returned relatively easily to the gas in the warmer regions of the disk.

The ionization fraction, $x(e)$, is an important parameter in disk modeling, possibly controlling the turbulence in a disk. Ceccarelli et al. (2004) observed H_2D^+ in several T Tauri stars and from this estimated the value of $x(e)$ in the midplane to be 7×10^{-10} in DM Tau, 4×10^{-10} in TW Hya and $< 2 \times 10^{-9}$ in LkCa 15. (H_3^+ and its deuterated isotopes are likely to major carriers of charge in the midplane where the high densities and low temperatures mean that other molecular ions e.g. HCO^+ are heavily depleted). Our results find a value $x(e) \sim$ a few $\times 10^{-10}$ in the outer disk midplane, with the exact value depending on the radius. This is consistent with the observed values for DM Tau and TW Hya but a little lower than that estimated for LkCa15. We find that the inclusion of diffusion does not affect $x(e)$ and that the major charge carriers in the midplane are the ions of atomic and molecular hydrogen (H^+ and H_3^+).

We find that our static ($K = 0 \text{ cm}^2\text{s}^{-1}$) models cannot keep sufficient molecules in the gas phase to account for the observed column densities without the inclusion of additional diffusion processes such as photodesorption. This result is a consequence of the relatively cool disk model we use for the density and temperature distributions (Aikawa et al. (2002) use a warmer disk model which permits the efficient thermal desorption of volatile molecules, and find much higher column densities as a result). The cooler models predict spectral energy distributions that are in better agreement with the observed T Tauri disks, but cause problems for the understanding of the chemistry. For example, observations of DM Tau find $N(\text{CO}) = 5.7 \times 10^{16} \text{ cm}^{-2}$ and $N(\text{CO})$ is even higher in LkCa 15 where $N(\text{CO}) = 1.6 \times 10^{18} \text{ cm}^{-2}$. Our $K = 0 \text{ cm}^2\text{s}^{-1}$ model predicts $N(\text{CO}) = 7.3 \times 10^{14} \text{ cm}^{-2}$ at $R = 300$ AU, considerably less than either observed value. The inclusion of diffusion with $K = 10^{18} \text{ cm}^2\text{s}^{-1}$ is sufficient to provide a means of keeping molecules in the gas while using the cool disks that produce better agreement with SEDs, and without the need to invoke alternative non-thermal desorption processes.

6. Effect of binding energy of CO on the results

In the previous section we presented the results of models that used a value of 1210 K for the binding energy of CO (Tielens & Allamandola 1987). Recent experimental work by Öberg et al. (2005) has suggested that $E_b(\text{CO})$ is actually considerably lower and, at 855 K, is close to that of N_2 . This would mean that CO could be more easily returned to the gas phase by thermal desorption. Since the chemistry is very dependent on the efficiency of thermal desorption, a change of this magnitude in the binding energy of a molecule could greatly change the gas phase chemistry.

To test how this affects our results we ran models at 100 AU and 300 AU using $\text{BE}(\text{CO})$

= 855 K. As expected, decreasing the CO binding energy increases the gas phase column density of CO at 100 AU from $1.9 \times 10^{15} \text{ cm}^{-2}$ to $2.4 \times 10^{17} \text{ cm}^{-2}$ for a model without mixing. When mixing with $K = 10^{18} \text{ cm}^2\text{s}^{-1}$ is included, the change in $E_b(\text{CO})$ increase $N(\text{CO})$ from 4.4×10^{16} to $2.9 \times 10^{17} \text{ cm}^{-2}$. The increase is due to the thermal desorption of CO from grains, which can now occur at lower temperatures ($\sim 17 \text{ K}$), resulting in a higher abundance in the midplane. At larger radii the change in $E_b(\text{CO})$ has less effect as the temperatures in the midplane are sufficiently cold that thermal desorption is not so important. Hence at $R = 300 \text{ AU}$ the change in $E_b(\text{CO})$ does not affect the CO column density for $K = 0$ and only results in an increase of a factor of 2 for the model with $K = 10^{18} \text{ cm}^2\text{s}^{-1}$.

Most other molecules are not affected by the presence of extra CO in the gas, but N_2H^+ shows a drop in column density due its destruction by reaction with CO in the midplane. (In models with a higher $E_b(\text{CO})$, where the midplane CO abundance is low, N_2H^+ is destroyed mainly by recombination with electrons). At $R < 100 \text{ AU}$, therefore, N_2H^+ will not trace the midplane if the CO binding energy is low, but it will be a possible tracer of this region at larger radii, where CO is accreted onto grains.

7. Discussion and conclusions

The inclusion of diffusion can have a considerable effect on model abundances, with the effect depending on the magnitude of the diffusion coefficient assumed. Diffusion tends to smooth out the vertical abundance gradients and to increase the vertical range over which molecules are present. Mixing transports atoms and ions from the surface photodissociation region into the molecular layer where they can be incorporated into new molecules. The transport of icy grains into warmer regions also affects the abundances of some (more volatile) molecules and is most effective at $R = 100 \text{ AU}$, where the greatest increase in column density with K is seen. Our models show that if $K < 10^{16} \text{ cm}^2\text{s}^{-1}$ then diffusion is unlikely to have much effect, except at small radii ($R = 100 \text{ AU}$). Diffusion does not destroy the three layer chemical structure of the disk predicted by static models, although the thickness of the molecular layer does increase.

We find that the inclusion of diffusive mixing can greatly affect the abundance of many species. Most molecules show an increase in column density, but some nitrogen-bearing molecules are decreased. How the column density is affected is related to the location of the molecules in the disk. Molecules that have their peak abundance at or near the midplane, e.g. N_2H^+ and NH_3 , are relatively unaffected by diffusion, whereas molecules which exist mainly in the molecular layer show increases in column density. This increase depends on

the magnitude of K , with higher values of K resulting in larger column densities.

Our calculated midplane ionization fraction is consistent with the observations of Ceccarelli et al. (2004), but do not change with the addition of diffusion.

In conclusion our models show that diffusion can greatly affect the chemistry in a disk. It is important to include the interplay of chemistry and dynamics in disks since both can have an effect on the other: the dynamics can change the abundance and distribution of many molecules and the chemistry can affect the ionization fraction, which in turn can determine whether or not the magneto-rotational instability can drive turbulence.

A. The species set

Gaseous species

H	H ₂	H ⁺	H ₂ ⁺	H ₃ ⁺	He	He ⁺	C	C ⁺	C ₂
C ₂ ⁺	O	O ⁺	O ₂	O ₂ ⁺	N	N ⁺	N ₂	N ₂ ⁺	Si
Si ⁺	CH	CH ₂	CH ₃	CH ₄	CH ⁺	CH ₂ ⁺	CH ₃ ⁺	CH ₄ ⁺	CH ₅ ⁺
C ₂ H	C ₂ H ⁺	C ₂ H ₂	C ₂ H ₂ ⁺	C ₂ H ₃ ⁺	C ₂ H ₄ ⁺	C ₃ ⁺	C ₃ H ⁺	C ₃ H ₃ ⁺	CO
CO ₂	CO ⁺	CO ₂ ⁺	HCO	HCO ⁺	H ₂ CO	H ₂ CO ⁺	H ₃ CO ⁺	HCO ₂ ⁺	CH ₃ OH
CH ₃ OH ₂ ⁺	OH	H ₂ O	OH ⁺	H ₂ O ⁺	H ₃ O ⁺	NH	NH ₂	NH ₃	NH ⁺
NH ₂ ⁺	NH ₃ ⁺	NH ₄ ⁺	N ₂ H ⁺	CN	HCN	HNC	CN ⁺	HCN ⁺	HCNH ⁺
CNC ⁺	C ₂ N ⁺	H ₂ NC ⁺	HC ₃ N	CH ₃ CN	H ₂ C ₃ N ⁺	H ₄ C ₂ N ⁺	NO	NO ⁺	e ⁻

Mantle species

H	H ₂	C	C ₂	O	O ₂	N	N ₂	Si	CH
CH ₂	CH ₃	CH ₄	C ₂ H	C ₂ H ₂	CO	CO ₂	HCO	H ₂ CO	CH ₃ OH
OH	H ₂ O	NH	NH ₂	NH ₃	CN	HCN	HNC	HC ₃ N	CH ₃ CN
NO									

This research was conducted at the Jet Propulsion Laboratory, California Institute of Technology under contract with the National Aeronautics and Space Administration. Partial support was provided by a grant from the NASA Origins Program.

REFERENCES

Aikawa, Y., & Herbst, E. 1999, A&A, 351, 223

- . 2001, *A&A*, 371, 1107
- Aikawa, Y., Momose, M., Thi, W.-F., van Zadelhoff, G.-J., Qi, C., Blake, G. A., & van Dishoeck, E. F. 2003, *PASJ*, 55, 11
- Aikawa, Y., Umebayashi, T., Nakano, T., & Miyama, S. 1999, *ApJ*, 519, 705
- Aikawa, Y., van Zadelhoff, G. J., van Dishoeck, E. F., & Herbst, E. 2002, *A&A*, 386, 622
- Allen, M., Yung, Y., & Waters, J. 1981, *J. Geophys. Res.*, 86, 3617
- Balbus, S. A., & Hawley, J. F. 1991, *ApJ*, 376, 214
- Balbus, S. A., Hawley, J. F., & Stone, J. M. 1996, *ApJ*, 467, 76
- Bauer, I., Finocchi, F., Duschl, W., Gail, H.-P., & Schlöder, J. 1997, *A&A*, 317, 273
- Beckwith, S., Sargent, A., Chini, R., & Guesten, R. 1990, *AJ*, 99, 924
- Bergin, E., Calvet, N., d'Alessio, P., & Herczeg, G. J. 2003, *ApJ*, 591, 159
- Bryden, G. A., Lin, D. N. C., Yorke, H. W., & Velusamy, T. 2006, in preparation
- Calvet, N., Hartmann, L., & Strom, S. E. 2000, in *Protostars and Planets IV*, ed. V. Mannings, A. Boss, & S. S. Russell (Tucson: University of Arizona Press), 377
- Carbadillo, A., Stone, J. M., & Pringle, J. E. 2005, *MNRAS*, 358, 1055
- Caselli, P., Hasegawa, T. I., & Herbst, E. 1998, *ApJ*, 495, 309
- Ceccarelli, C., Dominik, C., Lefloch, B., Caselli, P., & Caux, E. 2004, *ApJ*, 607, 51
- Charnley, S. B. 1997, in *IAU Colloq. 161: Astronomical and Biochemical Origins and the Search for Life in the Universe*, 89
- Chiang, E. I., & Goldreich, P. 1997, *ApJ*, 490, 368
- d'Alessio, P., Calvet, N., & Hartmann, L. 2001, *ApJ*, 553, 321
- d'Alessio, P., Calvet, N., Hartmann, L., Lizano, S., & Canto, L. 1999, *ApJ*, 527, 893
- Drouart, A., Dubrulle, B., Gautier, D., & Robert, F. 1999, *Icarus*, 140, 129
- Dubrulle, B., Marié, L., Normand, C., Richard, D., Hersant, F., & Zahn, J.-P. 2005, *A&A*, 429, 1

- Duschl, W., Gail, H.-P., & Tscharnuter, W. 1996, *A&A*, 312, 624
- Dutrey, A., Guilloteau, S., & Guélin, M. 1997, *Astron. Astrophys. Lett.*, 317, 5
- Finocchi, F., & Gail, H.-P. 1997, *A&A*, 327, 825
- Finocchi, F., Gail, H.-P., & Duschl, W. 1997, *A&A*, 325, 1264
- Gail, H.-P. 2001, *A&A*, 378, 192
- Guilloteau, S., & Dutrey, A. 1998, *A&A*, 369, 467
- Hammer, M. 1999, *Space Sci. Rev.*, 90, 99
- Hartmann, L., Calvet, N., Gullbring, E., & d'Alessio, P. 1998, *ApJ*, 495, 385
- Hasegawa, T. I., & Herbst, E. 1993, *MNRAS*, 261, 83
- Herbig, G. H., & Goodrich, R. W. 1996, *ApJ*, 309, 294
- Hiraoka, K., Sato, T., Sato, S., Sogoshi, N., Yokoyama, T., Takashima, H., & Kitagawa, S. 2002, *ApJ*, 577, 265
- Igea, J., & Glassgold, A. E. 1999, *ApJ*, 518, 848
- Ilgner, M., Henning, T., Markwick, A. J., & Millar, T. J. 2004, *A&A*, 415, 643
- Johansen, A., & Klahr, H. H. 2005, *ApJ*, 00, 00
- Kamp, I., & Dullemond, C.-P. 2004, *ApJ*, 615, 991
- Kastner, J. H., Huenemoerder, D. P., Schulz, N. S., Canizares, C. R., & Weintraub, D. A. 2002, *ApJ*, 567, 434
- Katz, N., Furman, I., Biham, O., Pirronello, V., & Vidali, G. 1999, *ApJ*, 522, 305
- Klahr, H. H. 2004, *ApJ*, 606, 1070
- Klahr, H. H., & Bodenheimer, P. 2003, *ApJ*, 582, 869
- Lee, H.-H., Herbst, E., Pineau des Forets, G., Roueff, E., & Le Bourlot, J. 1996, *A&A*, 311, 690
- Li, H., Finn, J. M., Lovelace, R. V. E., & Colgate, S. A. 2000, *ApJ*, 553, 1023
- Lin, D. N. C., & Papaloizou, J. 1980, *MNRAS*, 191, 37

- Markwick, A. J., Ilgner, M., Millar, T. J., & Henning, T. 2002, *A&A*, 385, 632
- Millar, T. J., Farquhar, P. R. A., & Willacy, K. 1998, *A&AS*, 121, 139
- Morfill, G. E. 1983, *Icarus*, 53, 41
- Morfill, G. E., & Völk, H. J. 1984, *ApJ*, 287, 371
- Muzerolle, J., Calvet, N., Briceno, C., Hartmann, L., & Hollenbrand, L. 2000, *ApJ*, 535, 47
- Öberg, K. I., van Broekhuizen, F., Fraser, H. J., Bisschop, S. E., van Dishoeck, E. F., & Schlemmer, S. 2005, *ApJ*, 621, L33
- Pollack, J. B., Hollenbach, D., Beckwith, S., Simonelli, D. P., Roush, T., & Fong, W. 1994, *ApJ*, 421, 615
- Prasad, S. S., & Tarafdar, S. P. 1983, *ApJ*, 267, 603
- Qi, C. 2001, PhD thesis, California Institute of Technology
- Richtmeyer, R. 1957, *Difference methods for initial-value problems* (New York, Interscience Publishers)
- Ruffle, D. P., & Herbst, E. 2000, *MNRAS*, 319, 837
- Sandford, S. A., & Allamandola, L. J. 1988, *Icarus*, 76, 201
- . 1990, *Icarus*, 87, 188
- . 1993, *ApJ*, 417, 815
- Shakura, N. I., & Sunyaev, R. A. 1973, *A&A*, 24, 337
- Shalybkov, D., & Rüdiger, G. 2005, *A&A*, 438, 411
- Shu, F. 1995, in *Molecular clouds and star formation*, ed. C. Yuan & J. H. You, *Proceedings of 7th Guo Shouying summer school on astrophysics* (Singapore: World Scientific), 97
- Simon, M., Dutrey, A., & Guilloteau, S. 2000, *ApJ*, 545, 1034
- Skrutskie, M., Dutkevitch, D., Strom, S., Edwards, S., Strom, K., & Stiwe, M. 1990, *AJ*, 99, 1187
- Stevenson, D. J. 1990, *ApJ*, 348, 730
- Strobel, D. F., & McElroy, M. B. 1970, *Planet. Space. Sci*, 18, 11811

- Strom, K., Strom, S., Edwards, S., Cabrit, S., & Skrutskie, M. F. 1989, *AJ*, 97, 1451
- Strom, S., Edwards, S., & Skrutskie, M. 1993, in *Protostars and Planets III*, ed. E. H. Levy & J. I. Lunine (Tucson: University of Arizona Press), 837
- Thi, W. F., van Dishoeck, E. F., Blake, G. A., van Zadelhoff, G. J., Horn, J., Becklin, E. E., Mannings, V., Sargent, A. I., van den Ancker, M. E., Natta, A., & Kessler, J. 2001, *ApJ*, 561, 1074
- Thi, W.-F., van Zadelhoff, G.-J., & van Dishoeck, E. F. 2004, *A&A*, 425, 955
- Tielens, A. G. G. M., & Allamandola, L. J. 1987, in *Physical processes in interstellar clouds*, ed. G. E. Morfill & M. Schöler (Dordrecht: Reidel), 333
- Tielens, A. G. G. M., & Charnley, S. B. 1997, *Origins of Life and Evolution of the Biosphere*, 27, 23
- Tielens, A. G. G. M., & Hagen, W. 1982, *A&A*, 114, 245
- Umebayashi, T., & Nakano, T. 1980, *PASJ*, 32, 405
- . 1981, *PASJ*, 33, 617
- Watanabe, N., & Kouchi, A. 2002, *ApJ*, 571, 173
- Webb, R. A., Zuckerman, B., Platais, I., Patience, J., White, R. J., Schwartz, M. J., & McCarthy, C. 1999, *ApJ*, 512, 63
- Wehrstedt, M., & Gail, H. P. 2002, *A&A*, 385, 181
- Willacy, K., Klahr, H. H., Millar, T. J., & Henning, T. 1998, *A&A*, 338, 995
- Willacy, K., & Langer, W. D. 2000, *ApJ*, 544, 903
- Willacy, K., Langer, W. D., & Allen, M. 2002, *ApJ*, 573, 119
- Willacy, K., Langer, W. D., & Bryden, G. C. 2006, *in prepration*
- Xie, T., Allen, M., & Langer, W. D. 1995, *ApJ*, 440, 674

Table 1. The input abundances for the molecular cloud model. Since a protoplanetary disk forms from material that has been processed in a molecular cloud, we use the outputs from the cloud model at 1 Myrs to provide the input abundances for the disk model. These are listed in Table 2.

Element	Fractional abundance
H ₂	0.99
H	0.01
He	0.14
O	1.76×10^{-4}
C ⁺	7.3×10^{-5}
N	2.14×10^{-4}
Si	2.0×10^{-8}

Table 2. Initial abundances as calculated in a molecular cloud model. a (b) indicates $a \times 10^b$.

Species	Fractional abundance	
	Gas	Grain
CO	6.2 (-6)	6.0 (-5)
CO ₂	1.3 (-8)	2.4 (-7)
H ₂ CO	3.8 (-8)	1.3 (-9)
O ₂	6.0 (-9)	1.3 (-5)
H ₂ O	1.5 (-7)	7.5 (-5)
CH ₄	1.6 (-7)	5.3 (-7)
C ₂ H	1.1 (-8)	
C ₂ H ₂	7.9 (-8)	1.6 (-6)
CN	3.0 (-8)	
HNC	2.7 (-8)	7.2 (-7)
HCN	4.2 (-8)	6.0 (-7)
HC ₃ N	6.0 (-8)	3.7 (-7)
NH ₃	1.7 (-9)	5.3 (-6)
N ₂	4.8 (-6)	5.5 (-8)
CH ₃ CN	1.7 (-9)	8.2 (-9)
CH ₃ OH	1.6 (-10)	
N	2.8 (-7)	
O	2.2 (-6)	
HCO ⁺	7.6 (-10)	
N ₂ H ⁺	5.0 (-10)	

Table 3. The binding energies (E_b) used to determine the thermal desorption rates of the abundant mantle species. References are (1) Sandford & Allamandola (1993), (2) Sandford & Allamandola (1990), (3) Sandford & Allamandola (1988), (4) Tielens & Allamandola (1987), (5) Ruffle & Herbst (2000)

Species	Binding Energy (K)	Reference
H	373	5
C	800	4
N	800	4
O	800	4
CO	1210	4
CO ₂	2860	2
H ₂ O	4820	3
NH ₃	3080	2
H ₂ CO	1760	4
CH ₃ OH	4240	1
H ₂	315	5
N ₂	710	4
O ₂	1210	4

Table 4. Calculated column densities (cm^{-2}) at 1 Myrs at $R = 300$ AU. $a(b)$ represents $a \times 10^b$. The observed values are taken from (1) Aikawa et al. (2002) (derived from Dutrey et al. (1997)), (2) Qi (2001) (3) Thi et al. (2004), (4) Aikawa et al. (2003). The column densities for LkCa 15 calculated from the single dish observations assume that the disk has a radius of 450 AU. For TW Hya the disk is assumed to be 165 AU in radius.

Molecule	$K = 0$	$K = 10^{18}$	DM Tau ¹	LkCa 15		TW Hya ³
	(cm^2s^{-1})	(cm^2s^{-1})		Interferometer ²	Single dish ³	
H ₂	1.1 (23)	1.1 (23)				
CO	7.3 (14)	1.3 (16)	5.7 (16)		1.9 (16)	3.2 (16)
HCN	1.4 (9)	6.6 (11)	2.1 (12)	2.4 (13)	1.8 (12)	9.7 (12)
HNC	1.1 (10)	8.8 (11)	9.1 (11)	< 5.4 (12)		< 1.4 (12)
CN	4.4 (11)	4.0 (13)	9.5 - 12 (12)	9.7 - 25 (13)	1.5 (13)	6.6 (13)
CH ₃ OH	1.9 (5)	2.5 (8)		7.3 - 18 (14)	< 7.1 (13)	< 1.1 (13)
H ₂ CO	2.9 (10)	7.1 (12)	7.6 - 19 (11)	7.2 - 19 (12) ⁴	7.1 - 51 (11)	< 8.0 (11)
HCO ⁺	5.9 (9)	2.4 (11)	4.6 - 28 (11)	1.5 (13)	3.3 (11)	4.4 (12)
H ₂ O	6.0 (10)	3.2 (12)				
C ₂ H	1.1 (12)	7.4 (13)	4.2 (13)			
N ₂ H ⁺	3.1 (11)	1.6 (11)	< 7.6 (11)		< 1.4 (12)	< 1.0 (13)
NH ₃	2.6 (12)	6.5 (11)				